Calibration Steering Laws to Estimate the Optical Properties of NASA's ACS3 Solar Sail

Livio Carzana[(1)], Andrea Minervino Amodio[(1)], Pieter Visser[(1)], W. Keats Wilkie[(2)], and Jeannette Heiligers[(1)]

[(1)] *Faculty of Aerospace Engineering, Delft University of Technology, Delft, The Netherlands*
Corresponding author's email: l.carzana@tudelft.nl

[(2)] *Langley Research Center, National Aeronautics and Space Administration, Hampton, USA*

NASA's ACS3 mission will be the first Earth-bound solar-sail mission to fly so-called calibration steering laws. These steering laws are designed to expose the sailcraft to a variety of dynamical conditions to isolate the effects of different parameters on the dynamics, thereby facilitating the estimation of these parameters. This paper presents the set of candidate calibration steering laws of ACS3, highlighting their operational challenges and impact on the estimation of the sail's reflectivity and specularity. The results show that, for a conservative GPS position accuracy of 10 m, accurate estimation of the reflectivity and specularity with uncertainties in the order of $10^{-4} - 10^{-3}$ can be achieved by flying any of the proposed calibration laws. However, ACS3's calibration steering laws were also found to introduce operational challenges that may hinder their implementation for extended periods of time. In particular, the decreased power generation capability of solar arrays was found to be the most severe operational challenge for two out of the five ACS3's calibration laws analysed.

I. Introduction

Solar sailing is a propulsion system that uses the solar radiation pressure (SRP) exerted on a thin, lightweight sail to produce thrust. Its propellantless nature makes it an attractive alternative to traditional low-thrust chemical propulsion. This has led to several studies assessing its potential for a variety of applications, including Earth-bound, interplanetary, and even inter-stellar missions [1, 2]. Despite the abundance of research on solar-sail orbital dynamics and control, the technological readiness level of solar sailing is currently limited due to several practical challenges [3]. These include the sail's manufacturing, its in-orbit deployment, and attitude control. For this reason, the majority of solar sails launched to date have been technology demonstrators whose objective was to assess the sails' deployment and orbit-changing capabilities. Among these are the recently flown Gama Alpha and Lightsail-2 missions from Gama and The Planetary Society, respectively [4]. Similarly, even more missions are scheduled for launch in the near future, including NASA's Advanced Composite Solar Sail System (ACS3) mission [5]. ACS3 will serve as sail-deployment technology demonstrator, but unlike the other solar-sail missions launched so far, it will be the first sailcraft to fly calibration steering laws. These steering laws are designed to isolate specific contributions to the sailcraft acceleration, in particular, the SRP, planerary radiation pressure (PRP), and aerodynamic accelerations. The use of calibration laws facilitates the in-orbit estimation of different parameters governing the aforementioned accelerations, thus allowing the refinement of the current state-of-the-art solar-sail acceleration models.

Despite their potential to increase the reliability of solar-sail technology, studies on calibration control laws have been conducted only in Ref. [6] to a preliminary extent. In light of this, this paper provides the first in-depth analysis of the estimation capacity of calibration control laws. The paper focuses on the set of candidate calibration steering laws that ACS3 might use, also highlighting the potential operational challenges they entail. First, the equations of motion of ACS3 are introduced, along with a detailed description of the acceleration models used. The calibration laws are then discussed and an analysis is presented to assess their operational challenges. Next, a covariance analysis is presented, illustrating the accuracy to which ACS3's optical coefficients can be estimated from GPS measurements. Finally, the conclusions of the study are given.

II. Dynamics

The dynamics of ACS3 are described in an Earth-centered inertial (ECI) reference frame $I(x, y, z)$, with the x-axis pointing towards the mean vernal equinox at January 1$^{\text{st}}$, 2000, the z-axis directed perpendicular to the mean equatorial plane at January 1$^{\text{st}}$, 2000 and pointing towards the Northern hemisphere, and the y-axis completing the right-handed frame. Within this frame, the equations of motion can be expressed in vectorial form as:

$$\ddot{\boldsymbol{r}} = \nabla U_{\oplus} + \boldsymbol{a}_{\odot} + \boldsymbol{a}_{\leftmoon} + \boldsymbol{a}_{aero} + \boldsymbol{a}_{SRP} + \boldsymbol{a}_{PRP} \quad (1)$$

In the above equation, $\boldsymbol{r}$ denotes the orbital position vector and the overhead dot notation indicates differentiation with respect to time. The Earth's gravitational acceleration

is represented by the term $\nabla U_\oplus$, with ∇ the gradient operator and $U_\oplus$ the Earth's gravitational potential defined using the spherical harmonic expansion of the gravity field as per Ref. [7]. $\boldsymbol{a}_\odot$ and $\boldsymbol{a}_\leftmoon$ indicate the point-mass solar and lunar gravitational accelerations. The aerodynamic acceleration, $\boldsymbol{a}_{aero}$, is modelled using the flat-plate hyperthermal free-molecular flow model as per Ref. [8], similar to other works that describe the aerodynamics of solar sails in the atmosphere [9–11]. The aerodynamic acceleration is computed using the NRLMSISE-00 atmospheric density model [12] with indices of solar radio flux at 10.7 cm and geomagnetic activity relative to the 50^{th} percentile retrieved from the Marshall Space Flight Center's forecast of February 2024 [13]. The SRP and PRP accelerations are denoted by $\boldsymbol{a}_{SRP}$ and $\boldsymbol{a}_{PRP}$, respectively. These accelerations are strictly related to the optical characteristics of the sail which, as will be seen in Section IV.II, are the key parameters in the estimation process. Therefore, a detailed presentation of their definitions is provided in the following subsections.

II.I Solar Radiation Pressure Acceleration

In this paper, the SRP acceleration is modelled assuming the sail to be flat and accounting for its optical properties, similar to the optical SRP acceleration model devised by McInnes in Ref. [14]. However, unlike McInnes' model, which assumes that only the sail's front side can be illuminated by sunlight, the model presented here accounts for the possibility that the sail's backside may also be illuminated. As shown in Section III, this can indeed occur for some calibration steering laws, which introduces the need to extend McInnes' optical SRP acceleration model.

The SRP acceleration is defined as:

$$\boldsymbol{a}_{\text{SRP}} = \nu \frac{2S_\oplus}{c}\frac{A}{m}\left(\frac{1\text{AU}}{s}\right)^2 |\cos\alpha|\{b_1\hat{\boldsymbol{s}} + (b_2|\cos\alpha| + b_3)\,\hat{\boldsymbol{n}}_{\boldsymbol{s}}\} \quad (2)$$

with ν the shadow factor computed through the conical shadow model of Ref. [7], $S_\oplus = 1361\,\text{W}/\text{m}^2$ the solar irradiance at one astronomical unit (AU) from the Sun [15], $c = 299792458$ m/s the speed of light in vacuum [16], A the sail area, m the sailcraft total mass, s the norm of the instantaneous Sun-to-sailcraft vector, $\boldsymbol{s}$, $\hat{\boldsymbol{s}} = \boldsymbol{s}/s$, and α denotes the pitch angle measured between $\hat{\boldsymbol{s}}$ and the sail normal direction pointing out from the sail's backside, $\hat{\boldsymbol{n}}$. The parameters b_1, b_2, and b_3 are defined as follows:

$$b_1 = \frac{1}{2}(1 - \tilde{r}_{sl}\,\tilde{s}_{sl}) \qquad b_2 = \tilde{r}_{sl}\,\tilde{s}_{sl}$$

$$b_3 = \frac{1}{2}\left(B_{sl}\,(1 - \tilde{r}_{sl}\,\tilde{s}_{sl}) + \text{sgn}(\cos\alpha)\,(1 - \tilde{r}_{sl})\,\frac{\varepsilon_f B_f - \varepsilon_b B_b}{\varepsilon_f + \varepsilon_b}\right)$$

with $\tilde{r}$, $\tilde{s}$, B, and ε denoting the reflectivity, specularity, non-Lambertian coefficient, and infrared emissivity of the sail, respectively, and the subscripts *"f"*, *"b"*, and *"sl"* indicating whether the optical coefficients of the sail's front side, back side, or sunlit side are considered. Depending on the sail orientation, the sunlit optical coefficients coincide either with those of the front or back side of the sail. In particular, these are correlated as follows:

$$\tilde{r}_{sl},\ \tilde{s}_{sl},\ B_{sl} = \begin{cases} \tilde{r}_f,\ \tilde{s}_f,\ B_f & \text{if } \text{sgn}(\cos\alpha) = 1 \\ \tilde{r}_b,\ \tilde{s}_b,\ B_b & \text{otherwise} \end{cases}$$

Ultimately, $\hat{\boldsymbol{n}}_{\boldsymbol{s}}$ represents the sail normal direction with no positive component towards the Sun, given by:

$$\hat{\boldsymbol{n}}_{\boldsymbol{s}} = \text{sgn}(\cos\alpha)\,\hat{\boldsymbol{n}}$$

II.II Planetary Radiation Pressure Acceleration

In this paper, the PRP acceleration is modelled as per the spherical optical PRP acceleration model presented in Ref. [17]. Similar to the optical SRP acceleration model, this PRP acceleration model also accounts for the sail's optical properties. However, a major difference between the two models exists, that is, the definitions of the radiation intensity and the associated radiation pressure exerted onto the sail. Indeed, planetary radiation originates from the Earth and its intensity depends on several factors, including the sailcraft's geographical location and altitude, and the illumination conditions of the Earth as seen from the sailcraft. Furthermore, because the sailcraft flies in close proximity of the Earth, planetary radiation can reach only the sail's front side, only its back side, or both sides simultaneously, depending on its orientation. For this reasons, the PRP acceleration depends on the optical coefficients of both sides of the sail in a highly non-linear manner, rendering its expression very elaborate. In light of this and for the sake of brevity, the full expression of the PRP acceleration will not be provided in this paper. For additional information on the model, its derivation and accuracy, the reader is referred to Ref. [17].

II.III ACS3 Properties

Table 1 provides the optical coefficients, aerodynamic coefficients, mass, and sail area of ACS3, which will be considered throughout the paper. The provided optical coefficients are valid for both the SRP and PRP accelerations. The aerodynamic coefficients are the sail's normal and transversal momentum exchange coefficients, σ_N and σ_T, respectively, and the ratio of the atmospheric particle average thermal velocity to the sailcraft inertial velocity, V_R. Apart from the above-mentioned parameters related to ACS3's dynamics, the table also gives information on ACS3's maximum achievable attitude rate of change, $\dot{\varphi}_{max}$, the expected sail deployment date, and the corresponding orbital elements at the time of deployment. The orbital elements are the semi-major axis, eccentricity, inclination, right ascension of the ascending node, argument of pericenter, and true anomaly, denoted by a, e, i, Ω, ω, and ϑ, respectively. The information presented in the table will be used as input to the analysis of the calibration steering laws and their estimation capability in the remainder of the paper.

Table 1: ACS3 mission specifics.

Spacecraft Specifications	
m	16 kg
A	80 m^2
$\dot{\varphi}_{max}$	0.5 deg/s
Frontside Optical Coefficients	
$\tilde{r}_f$	0.90
$\tilde{s}_f$	0.82
B_f	0.79
ε_f	0.03
Backside Optical Coefficients	
$\tilde{r}_b$	0.43
$\tilde{s}_b$	0.53
B_b	0.67
ε_b	0.60
Aerodynamic Coefficients	
σ_N	0.80
σ_T	0.80
V_R	0.05
Initial State in ECI Frame	
a	7378.1363 km
e	0
i	99.4793 deg
Ω	257.5333 deg
ω	0.0 deg
ϑ	0.0 deg
Sail Deployment Date	1 July 2024, 12:00 PM

III. Calibration Steering Laws

As discussed in Section II, Earth-orbiting sailcraft are subject to several accelerations that affect their dynamics. While the gravitational accelerations of the Earth and other celestial bodies only depend on the sailcraft position, other accelerations also depend on the sailcraft attitude, namely, the SRP, PRP, and aerodynamic accelerations. Due to this dependency, the magnitude and direction of these accelerations can be changed at will by controlling the sail's orientation, that is, by employing specific steering laws. The calibration steering laws are dedicated steering laws designed to amplify the aforementioned attitude-dependent accelerations, thus making their contributions to the total acceleration easier to isolate and identify. Designing such steering laws in an effective manner can be challenging for a variety of reasons. The primary challenge is given by the fact that changing the sailcraft attitude affects the SRP, PRP and aerodynamic accelerations simultaneously, making it intrinsically difficult to truly isolate the contribution of each acceleration. In addition, the extent to which a calibration law can calibrate the SRP, PRP, and aerodynamic accelerations depends on the specific orbit considered and, particularly, on its altitude and orientation with respect to the direction of sunlight. Finally, the design of the calibration steering laws should account for potential operational constraints, which can be particularly stringent for complex steering laws, specific orbit orientations, and limited sailcraft attitude-changing capabilities.

Taking the above into account, several discussions were held with the ACS3 mission team to determine the calibration steering laws that would maximize the calibration capacity of ACS3. As a result, five candidate calibration laws were shortlisted. These are presented in the following section, followed by an analysis of the operational challenges they entail.

III.I Definition

A steering law can be unambiguously defined by specifying the orientation of the sail's normal direction along the orbit. In light of this, the ACS3's candidate calibration steering laws are named after the target direction of the sail's normal. These are:

- **Backside nadir pointing**, see Figure 1, left. The normal to the sail's backside, $\hat{\boldsymbol{n}}$, points antiparallel to the radial direction, $\hat{\boldsymbol{r}}$, so that the sail is edgewise to the incoming atmospheric velocity and the backside always faces the Earth. It should be noted that since ACS3's antennas are mounted on the sailcraft backside, this calibration law also ensures optimal contact with the ground stations. Because of this property, this calibration law is the default steering law of ACS3 and will also be referred to as "standby" steering law in the following.

- **Frontside nadir pointing**. The normal direction, $\hat{\boldsymbol{n}}$, points parallel to the radial direction, $\hat{\boldsymbol{r}}$. Therefore, the sail's highly reflective frontside faces the Earth, thus yielding an even larger PRP acceleration compared to the backside nadir-pointing steering law.

- **Sun pointing**, see Figure 1, center. The normal direction, $\hat{\boldsymbol{n}}$, is constantly parallel to the sunlight direction, $\hat{\boldsymbol{s}}$, even when in eclipse. This results in $\alpha = 0$ and a maximum SRP acceleration all the time.

- **Drag pointing**, see Figure 1, right. The normal direction, $\hat{\boldsymbol{n}}$, points parallel to the inertial velocity, $\boldsymbol{v}$. In this way, the sail's frontside faces the incoming atmospheric particles, thus maximising atmospheric drag.

- **Fixed in-plane pointing**. The normal direction $\hat{\boldsymbol{n}}$ constantly points towards a pre-determined direction $\hat{\boldsymbol{d}}$ lying within the orbital plane. For ACS3, $\hat{\boldsymbol{d}}$ was cho-

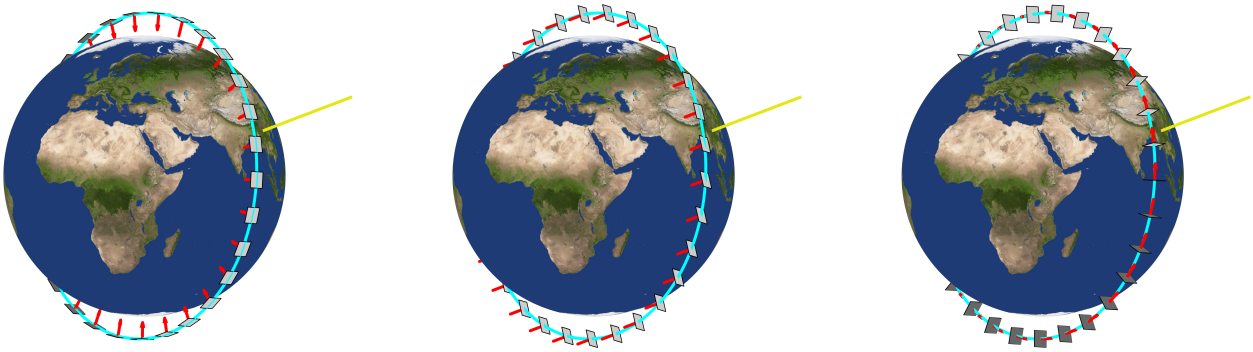

Figure 1: ACS3's backside nadir-pointing steering law (left), Sun-pointing steering law (center), and drag-pointing steering law (right). The light grey and dark grey squares represent the sail's front and back sides, respectively. The light blue curve, yellow arrow, and red arrows indicate ACS3's orbit, Earth-to-Sun direction, and sail normal directions, respectively.

sen as the in-plane direction forming the smallest angle with the sunlight direction $\hat{\boldsymbol{s}}$. Mathematically, this corresponds to:

$$\hat{\boldsymbol{d}} = \hat{\boldsymbol{h}} \times \frac{\hat{\boldsymbol{s}} \times \hat{\boldsymbol{h}}}{||\hat{\boldsymbol{s}} \times \hat{\boldsymbol{h}}||}$$

where $\hat{\boldsymbol{h}} = (\boldsymbol{r} \times \boldsymbol{v}) / ||\boldsymbol{r} \times \boldsymbol{v}||$ denotes the orbital momentum direction.

III.II Analyses

The steering laws presented in the previous section facilitate the calibration of the accelerations of ACS3. However, the implementation of these steering laws also poses operational challenges which may compromise their feasibility. This section aims to characterise the severity of these operational challenges and, therefore, assess the feasibility of each calibration law. The operational challenges considered in the analysis are the following:

- **Altitude decrease**. Employing the calibration steering laws for an extended period of time can yield undesirable changes in the sailcraft's orbital parameters and, particularly, in its altitude.
- **Sailcraft attitude rate of change**. Depending on the complexity of the steering law, the sailcraft may be required to change attitude rapidly, beyond the turning rates achievable by ACS3's reaction wheels (0.5 deg/s, see Table 1).
- **Solar sail's backside exposure to sunlight**. Solar sails usually feature a highly reflective, aluminium-coated front side, which helps maximise the sailcraft thrusting capabilities, whereas the backside is either uncoated or, as in the case of ACS3, coated with chromium. The chromium coating enhances the emissivity of the sail, which is crucial for thermal control [14, 18]. When sunlight – and especially ultraviolet – radiation illuminates the sail's backside, it causes rapid degradation of the sail material and thus its sail's optical properties and performance. Although the back of a solar sail is usually not illuminated by sunlight, some of the ACS3's calibration laws can yield temporary exposure of the sail's backside to sunlight.
- **Power generation**. The solar panels of ACS3 are mounted parallel to the sail plane, so that they generate power when the sail's front side is illuminated. Implementing some calibration steering laws can yield extended periods of time during which the solar arrays are oriented unfavourably, resulting in potential power generation issues.

The analysis presented in this section is fully based on ACS3's mission specifics. The initial state corresponds to the expected orbit insertion of the sailcraft, defined by the orbital elements of Table 1. These identify a circular, Sun-synchronous orbit with altitude of 1000 km and local time of the ascending node at 10:30 PM. The simulation start time is set to July 1^{st} 2024, i.e., the expected deployment date of the sail, see Table 1. For each calibration steering law presented in Section III.I, the dynamics given in Equation 1 are propagated neglecting solar and lunar gravity (i.e., $\boldsymbol{a}_{\odot}=\boldsymbol{a}_{\leftmoon}=\boldsymbol{0}$) and modelling the Earth's gravitational potential, $U_{\oplus}$, using spherical harmonics up to degree 2 and order 0, that is, only including the Earth's central gravity and J_2 gravity terms. The propagation uses the ACS3 specifics of Table 1 while enforcing the maximum attitude rate of change, $\dot{\varphi}_{max}$, of 0.5 deg/s. Finally, the propagation is performed using Matlab®'s *ode45* integrator for a simulation duration of 10 days, with absolute and relative tolerances set to 10^{-12}.

Table 2 presents the results of the analysis, providing information on the operational difficulties of each calibration steering law. The first two columns show the altitude loss per day and maximum rate of attitude change required by each steering law. The third column displays the amount of time during which the sail's backside is exposed to sunlight.

Table 2: Operational Challenges of ACS3's Calibration Steering Laws

Calibration Steering Law	**Altitude Loss** [km/day]	**Max. Attitude Rate of Change Required** [deg/s]	**Sail's Backside Exposure to Sunlight** [% Sunlit Orbital Period]	**Cumulative Flux on Solar Arrays** [% Max. Cum. Flux]
Backside Nadir Pointing	0.0	0.057	25.93	44.83
Frontside Nadir Pointing	0.0	0.057	74.05	6.73
Sun Pointing	0.113	0.0	0.0	100.0
Drag Pointing	0.175	0.057	49.83	34.38
Fixed In-plane Pointing	0.118	0.0	0.0	95.33

To make this parameter independent of eclipses – which last for approximately 32.5% of ACS3's orbital period – the exposure time is adimensionalised with respect to the total time ACS3 is illuminated by sunlight. Finally, the last column provides information on ACS3's power-generation capability. The latter is measured through the cumulative radiation flux captured by the solar arrays, which is proportional to the total power the solar arrays can generate. It should be noted that, in the table, the cumulative flux is adimensionalised with respect to the maximum cumulative flux ACS3's solar arrays can collect, i.e., the cumulative flux obtained when employing the Sun-pointing steering law. To highlight the benefits and drawbacks of each calibration law in relation to the operational challenges, the table uses a colour code with green representing the benefits, yellow indicating minor issues, and red indicating major problems.

The results show that the two nadir-pointing steering laws do not yield any change in altitude. This is because the sail is constantly oriented edgewise with respect to the velocity vector, which minimises atmospheric drag. The other steering laws yield only small altitude losses because the altitude of ACS3 is 1000 km, where atmospheric density is low. The table also shows that the required attitude change capabilities are well below ACSS'3 maximum achievable value of 0.5 deg/s. The exposure of the solar arrays and sail's backside to sunlight represents the most critical operational challenges for several calibration laws. For example, for the frontside nadir-pointing steering law, very little sunlight reaches the solar panels and the sail's backside is exposed to sunlight for extended periods of time. Similarly, the drag-pointing steering law is found to be challenging because of its limited power generation capability. The backside nadir-pointing steering law, on the other hand, achieves better performance. Indeed, the sail's backside is illuminated only during short periods of time, while the solar panels acquire almost 45% of the available solar power. Finally, the Sun-pointing and fixed in-plane pointing steering laws provide the best results, as the solar panels are constantly exposed to sunlight and the sail's backside is never illuminated.

The analysis presented in this section highlights how some operational constraints render the implementation of the calibration steering laws challenging. Nevertheless, these operational difficulties do not prevent the calibration laws from being employed altogether. Indeed, for successful calibration, these steering laws may only need to be implemented for a limited amount of time. Therefore, during this time, altitude loss, inability to generate power, and sail's material degradation caused by the sail's backside exposure to sunlight may be limited and not jeopardise the mission. To determine if this is the case, it is necessary to know the extent of time that each steering law needs to be sustained. In order to provide further insights into this problem, Section IV investigates the calibration capacity of each calibration steering law and assesses the corresponding time required to achieve a given calibration accuracy.

IV. Covariance Analysis

This section explores the achievable uncertainty levels in estimating ACS3's optical coefficients. For each calibration steering law presented in Section III.I, a covariance analysis is performed to estimate these uncertainties using simulated observations that mimic ACS3's GPS measurements.

The following subsections detail the methodology employed for the covariance analysis, including the covariance matrix generation, the selection and rationale behind the estimated parameters, and the observation acquisition scenarios used as input. Finally, the resulting formal uncertainties in the estimated optical coefficients are presented and recommendations for refining ACS3's operational planning are provided.

IV.I Covariance Matrix Generation

The covariance matrix $\boldsymbol{P}$ is computed as [7]:

$$\boldsymbol{P} = \left(\boldsymbol{H}^T \boldsymbol{W} \boldsymbol{H}\right)^{-1}$$

where $\boldsymbol{H}$ is the design matrix and $\boldsymbol{W}$ is the weight matrix of the observations. $\boldsymbol{H}$ contains the partial derivatives of the modelled observations $\boldsymbol{h}$ with respect to the set of parameters being estimated $\boldsymbol{q}$:

$$\boldsymbol{H} = \frac{\partial \boldsymbol{h}}{\partial \boldsymbol{q}}$$

Each element of $\boldsymbol{H}$ captures the effect of a small change in a particular parameter on a specific observation. The elements of the weight matrix of observations, $\boldsymbol{W}$, provide a statistical description of the random errors affecting the observations. Assuming N independent observations, $\boldsymbol{W}$ becomes a block diagonal matrix:

$$\boldsymbol{W} = \begin{bmatrix} \boldsymbol{W}_{11} & & \\ & \ddots & \\ & & \boldsymbol{W}_{NN} \end{bmatrix}$$

where the block $\boldsymbol{W}_{ii}$ represents the weight matrix of a single observation i. In addition, assuming the absence of correlations between the n different components of a single observation, $\boldsymbol{W}_{ii}$ is also diagonal:

$$\boldsymbol{W}_{ii} = \begin{bmatrix} \sigma_{11}^{-2} & & \\ & \ddots & \\ & & \sigma_{nn}^{-2} \end{bmatrix}$$

with σ_{kk}^2 denoting the Gaussian white noise variance of the k-th component of observation i.

The formal error σ_{q_j} represents the one-sigma formal uncertainty associated with the estimated parameter q_j and can be directly retrieved from the diagonal of the covariance matrix as:

$$\sigma_{q_j} = \sqrt{P_{jj}}$$

It is important to note that formal errors assume that the underlying dynamical and observational models used in the analysis are perfect. In reality, these models will have limitations, potentially causing the true errors in the estimated parameters to be larger than the formal errors indicate. While formal errors provide a valuable statistical representation of the quality of the parameter estimation, especially in the absence of flight data to validate the solution, they should be interpreted cautiously.

IV.II Estimated Parameters

To identify the most critical parameters to estimate, an analysis of the sensitivity of the SRP and PRP acceleration envelope curves to the sail optical coefficients is conducted. An acceleration envelope (AE) curve represents all potential accelerations achievable by the sailcraft when changing its attitude. As the SRP and PRP accelerations vary in both magnitude and direction with the sail attitude, distinct AE curves are defined for each.

This analysis focuses on the change in AE curves to a one-sigma uncertainty of 10%[1] in each optical coefficient listed in Table 1. This uncertainty accounts for potential experimental errors during ACS3's film material testing. The analysis evaluates the response to each coefficient individually for the case where the spacecraft's front side faces the radiation pressure source.

The results indicate that the frontside reflectivity and frontside specularity have the most significant influence on both the SRP and PRP accelerations, see Figure 2. Because the remaining coefficients exhibit minimal impact, with the nominal value curves practically overlapping the curves considering the one-sigma uncertainty, figures for those coefficients are not shown here. Consequently, frontside reflectivity and specularity are included in the set of parameters to be estimated alongside ACS3's initial state.

IV.III Observation Acquisition Scenarios

ACS3's GPS measurements are represented as three-dimensional Cartesian position observations. These observations are generated using the TU Delft Astrodynamics Toolbox (Tudat) software [19–21], which has been extended to incorporate the sailcraft dynamics presented in Equation 1. Earth's gravitational potential, $U_\oplus$, is modelled in Tudat using spherical harmonics up to degree and order 50. The simulation start time is set to July 1st, 2024, with the initial state defined by the orbital elements in Table 1. The observations are generated considering a noise with standard deviation σ_{kk} of 1 m. This choice does not affect the relative performance comparison between calibra-

[1]Uncertainty value taken from personal communication with J. Ho Kang, Advanced Materials and Processing Branch, NASA Langley Research Center, March 2024.

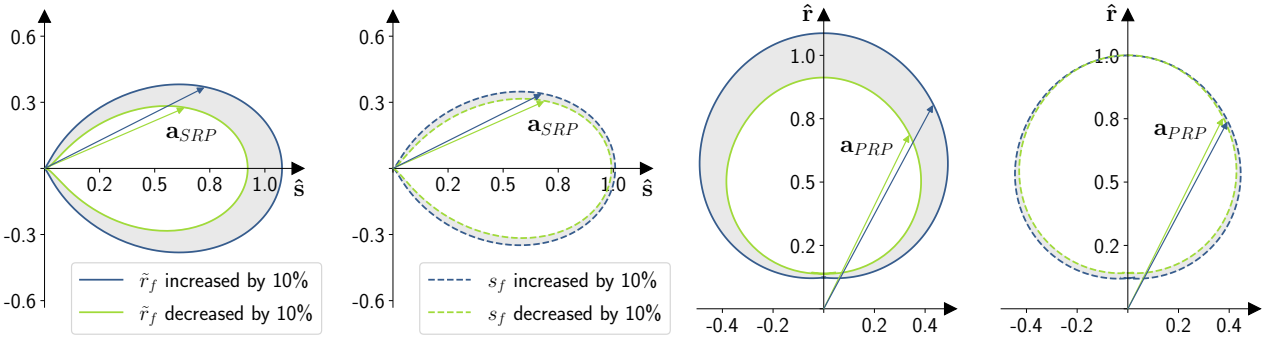

Figure 2: Change of the SRP and PRP acceleration envelope curves to a one-sigma variation of 10% in the sail's frontside reflectivity, $\tilde{r}_f$, and specularity, $\tilde{s}_f$. The acceleration envelope curves are normalised with respect to the maximum achievable SRP and PRP accelerations found for the nominal optical coefficients of Table 1.

tion laws. Due to the weight matrix being diagonal, the formal errors in the covariance matrix scale linearly with the inverse of any chosen standard deviation value.

To investigate the sensitivity of parameter uncertainties to data volume and density, the covariance matrix is computed for various combinations of observation windows and observation intervals. Based on discussions held with the ACS3 team, mission operation planning allows each candidate calibration steering laws to be flown for a maximum of 7 days. Consequently, the covariance analysis examines observation windows ranging from 1 orbit (approximately 105 minutes) to 98 orbits, with 14 orbits corresponding roughly to 1 day.

Furthermore, the analysis explores different observation intervals for the Cartesian measurements. While a typical GPS receiver for a low-Earth orbit (LEO) satellite has an update rate of 1 Hz, various factors can influence the observation frequency. Limited data storage capacity can necessitate smaller update rates (less frequent data recording) to keep the data volume manageable. Similarly, power consumption constraints may decrease the number of observations, as very frequent updates require more power. To account for potential operational limitations, the analysis considers intervals ranging from one observation per second to one observation per minute.

IV.IV Results

The formal uncertainties of ACS3's frontside reflectivity and specularity are estimated for each calibration steering law using the covariance analysis methodology described in Section IV.I. The results are presented in Figures 3 and 4. These contour plots provide the levels of the formal uncertainties expressed as a function of the observation noise standard deviation, σ_{obs}. This enables the interpretation of the formal uncertainties across a range of orbit determination accuracies.

Typical position accuracies from real-time GPS measurements range from 1 meter to 10 meters, while refined orbital solutions attainable via post-processing techniques can reach sub-centimetre levels. Since the achievable accuracy depends on various factors, including the receiver type, processing techniques, and additional data quality, a conservative scenario of a 10-meter observation noise level is considered for further discussion.

To increase the accuracy of current solar-sail dynamical models, the target formal error uncertainty should be in the $10^{-3}-10^{-4}$ interval. This range might appear particularly conservative when considering that the experimental uncertainty is within the $10^{-1}-10^{-2}$ range (see Section IV.II). However, the formal uncertainties obtained from the covariance analysis do not account for potential mismodeling in the spacecraft dynamics and observation models. Moreover, experimental uncertainty cannot account for changes in the sail's reflective, diffractive, or absorptive properties due to degradation in the harsh space environment or deployment imperfections (tears, wrinkles).

The comparison of the formal uncertainties across different calibration laws confirms the strong link between the number of observations and the achieved uncertainty level. A larger number of observations, achieved through either a higher frequency or a longer observation window (orbital revolutions), leads to smaller formal errors. In general,

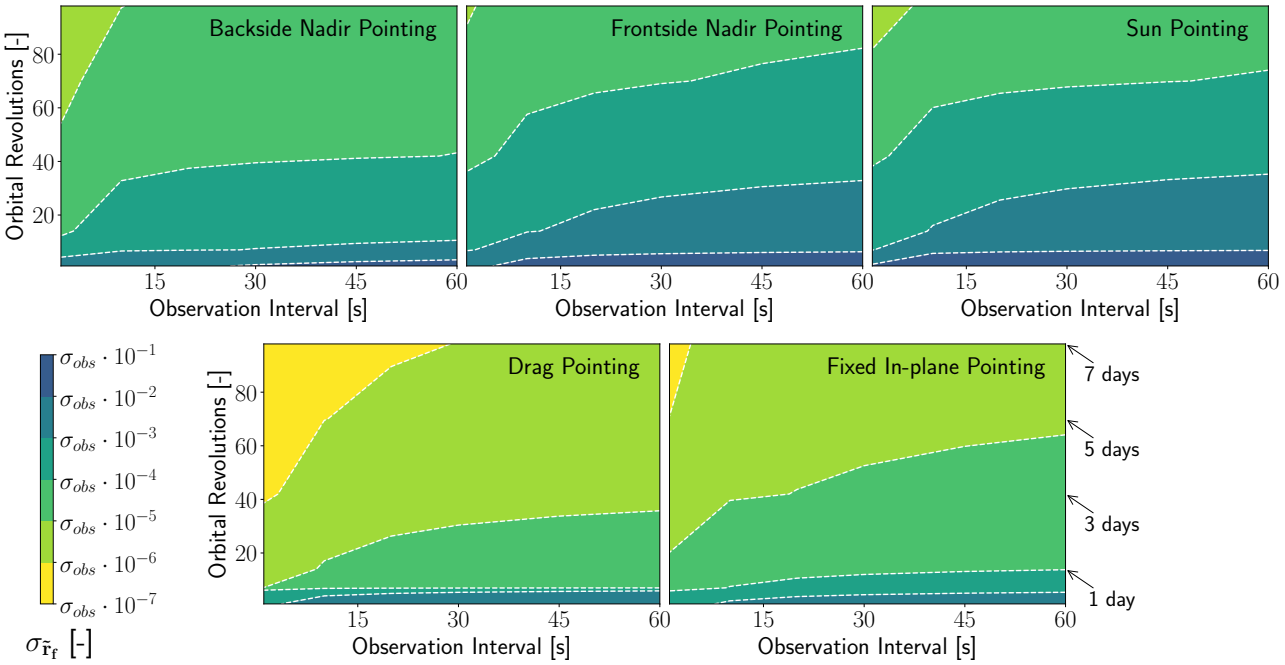

Figure 3: Formal uncertainties of ACS3's frontside reflectivity for different calibration steering laws.

more data points provide a more comprehensive picture of the system dynamics and constrain the solution space more effectively. Additionally, over extended observation periods, even subtle orbital changes become more significant, and the low-signal nature of SRP and PRP accelerations makes both frequent observations and longer observation windows crucial for capturing their effects.

Within the maximum seven-day window allowed for the calibration process, all candidate steering laws achieve the target uncertainty level of $10^{-3}-10^{-4}$. However, significant performance differences exist between them. Drag pointing and fixed-in-plane pointing outperform the other steering laws for reflectivity estimation, achieving the smallest formal errors. Backside nadir pointing followed by the fixed in-plane pointing and drag-pointing steering laws demonstrate the best performance for specularity estimation. While the frontside and backside nadir-pointing steering laws exhibit similar uncertainty levels for both reflectivity and specularity, the other calibration steering laws show that reflectivity can be estimated with smaller uncertainty. In general, changes in reflectivity have a more pronounced effect on the spacecraft's acceleration compared to specularity, especially when the sail is oriented perpendicular to the radiation source, as shown in Figure 2. This makes it easier to isolate and estimate the specific effect of reflectivity on the sailcraft's motion.

Analysing the Sun-pointing steering law provides additional insights into the complex non-linearity of the estimation problem. Despite benefitting from a constant and strong SRP signal, the Sun-pointing steering law performs poorly for both the reflectivity and specularity estimation. This is because the reflectivity and specularity become highly correlated in this configuration. Equation 2 illustrates this point. When substituting $\hat{\boldsymbol{n}} = \hat{\boldsymbol{s}}$ to the equation, all terms of the SRP acceleration act along the same direction, making it impossible to distinguish the individual effects of reflectivity and specularity on the sailcraft's motion. Consequently, the Sun-pointing calibration law relies on the less strong PRP acceleration signal to estimate these parameters, leading to higher uncertainties compared to the similarly defined fixed in-plane pointing. For the fixed in-plane pointing steering law, the angle between $\hat{\boldsymbol{n}}$ and $\hat{\boldsymbol{s}}$ remains constant at approximately 17 degrees. This separation allows the SRP signal to be used to decouple the individual effects of reflectivity and specularity, effectively leading to smaller formal uncertainties.

Finally, to address the possibility that calibration manoeuvres cannot be performed, it is worth mentioning that the standby backside nadir-pointing attitude can be effectively used for calibration purposes. It is recommended to maintain this attitude for at least 15 orbital revolutions if observations are provided every second or up to 45 revolutions for minute-interval observations. These recommendations hold for both the estimation of ACS3's reflectivity and specularity (see Figures 3 and 4).

V. Conclusions

This paper demonstrates that all ACS3's candidate calibration laws can significantly improve the accuracy of the sail optical coefficients compared to ground-based measurements. In particular, by flying any of ACS3's calibration

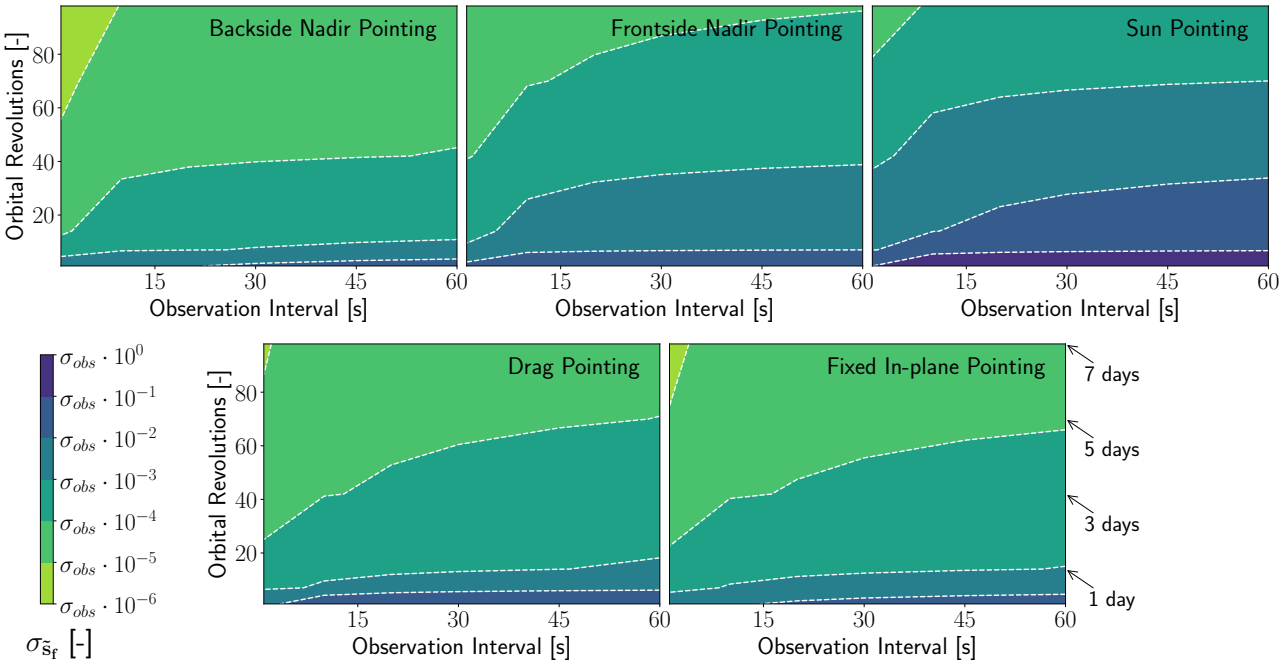

Figure 4: Formal uncertainties of ACS3's frontside specularity for different calibration steering laws.

laws for less than seven days, the uncertainties in reflectivity and specularity can be reduced by 2-3 orders of magnitude, assuming a conservative GPS position accuracy of 10 m. Despite this, calibration laws differ in both estimation performance and operational complexity. While the drag-pointing and fixed in-plane pointing steering laws offer superior accuracy in estimating the sail's frontside reflectivity, the drag-pointing steering law presents severe operational concerns due to the unfavourable orientation of the solar arrays along the orbit. On the other hand, the backside nadir-pointing and fixed in-plane pointing steering laws perform best to estimate the sail's frontside specularity, without introducing significant operational challenges. Since the backside nadir-pointing control law is ACS3's default steering law, this result is particularly convenient.

In light of the above, the backside nadir-pointing steering law offers a good balance between calibration performance and operational difficulties involved. Therefore, this steering law is deemed the most practical choice for ACS3's initial calibration. However, to increase the estimation accuracy even further, it is recommended to employ the fixed in-plane pointing steering law in subsequent calibration phases.

VI. Acknowledgements

Part of this work was funded by a Vidi Grant of the Dutch Research Council (NWO), Project Number 19690: SWEEP – Space Waste Elimination around Earth by Photon Propulsion. The authors would also like to thank D. Dirkx and M. S. Fayolle from the Department of Space Engineering at TU Delft for their invaluable insights regarding orbit determination aspects and the use of the Tudat software.

VII. References

[1] P. Zhao, C. Wu, and Y. Li. "Design and application of solar sailing: A review on key technologies". *Chinese Journal of Aeronautics*, vol. 36, no. 5, pp. 125–144, 2023.

[2] M. Macdonald and C. McInnes. "Solar sail science mission applications and advancement". *Advances in Space Research*, vol. 48, no. 11, pp. 1702–1716, 2011.

[3] D. A. Spencer, L. Johnson, and A. C. Long. "Solar sailing technology challenges". *Aerospace Science and Technology*, vol. 93, p. 105276, 2019.

[4] D. A. Spencer, B. Betts, J. M. Bellardo, A. Diaz, B. Plante, and J. R. Mansell. "The Lightsail 2 solar sailing technology demonstration". *Advances in Space Research*, vol. 67, no. 9, pp. 2878–2889, 2021.

[5] W. K. Wilkie, J. M. Fernandez, O. R. Stohlman, N. R. Schneider, G. D. Dean, J. Ho Kang, J. E. Warren, S. M. Cook, P. L. Brown, T. C. Denkins, S. D. Horner, E. D. Tapio, M. Straubel, M. Richter, and J. Heiligers. "Overview of the NASA Advanced Composite Solar Sail System (ACS3) technology demonstration project". In *AIAA Scitech 2021 Forum*, pp. 1–23. American Institute of Aeronautics and Astronautics Inc. (AIAA), 2021.

[6] L. Carzana, W. K. Wilkie, A. Heaton, B. Diedrich, and J. Heiligers. "Solar-sail steering laws to calibrate the accelerations from solar radiation pressure, planetary radiation pressure, and aerodynamic drag". In *6th International Symposium on Space Sailing (ISSS 2023)*, pp. 58–65. New York, USA, 2023.

[7] O. Montenbruck and E. Gill. *Satellite Orbits: Models, Methods and Applications*. 1st ed. Berlin, Germany: Springer-Verlag, 2000.

[8] J. A. Storch. "Aerodynamic disturbances on spacecraft in free-molecular flow". Tech. Rep. TR-2003(3397)-1, The Aerospace Corporation, 2003.

[9] G. Mengali and A. A. Quarta. "Near-optimal solar-sail orbit-raising from low Earth orbit". *Journal of Spacecraft and Rockets*, vol. 42, no. 5, pp. 954–958, 2005.

[10] V. Stolbunov, M. Ceriotti, C. Colombo, and C. R. McInnes. "Optimal law for inclination change in an atmosphere through solar sailing". *Journal of Guidance, Control, and Dynamics*, vol. Vol. 36, no. 5, pp. 1310–1323, 2013.

[11] L. Carzana, P. N. A. M. Visser, and J. Heiligers. "Locally optimal control laws for Earth-bound solar sailing with atmospheric drag". *Aerospace Science and Technology*, vol. Vol. 127, p. 107666, 2022.

[12] J. M. Picone, A. E. Hedin, D. P. Drob, and A. C. Aikin. "NRLMSISE-00 empirical model of the atmosphere: Statistical comparisons and scientific issues". *Journal of Geophysical Research: Space Physics*, vol. 107, no. A12, pp. SIA 15–1–SIA 15–16, 2002.

[13] "NASA Marshall Space Flight Center's archived forecast", Accessed: 15 December 2021. URL `https://www.nasa.gov/msfcsolar/archivedforecast`.

[14] C. R. McInnes. *Solar Sailing: Technology, Dynamics and Mission Applications*. Chichester, England, U.K.: Springer-Verlag, 1999.

[15] K. L. Yeo, N. A. Krivova, and S. K. Solanki. "Solar cycle variation in solar irradiance". *Space Science Reviews*, vol. 186, pp. 137–167, 2014.

[16] J. R. Wertz, W. J. Larson, D. Kirkpatrick, and D. Klungle. *Space mission analysis and design*, vol. 8. Springer, 1999.

[17] L. Carzana, P. Visser, and J. Heiligers. "A new model for the planetary radiation pressure acceleration for optical solar sails". In *6th International Symposium on Space Sailing (ISSS 2023)*, pp. 97–104. New York, USA, 2023.

[18] J. Ho Kang, K. L. Gordon, R. G. Bryant, O. R. Stohlman, W. K. Wilkie, A. E. Stark, R. S. Barfield, B. R. Sindle, M. M. Finckenor, and P. D. Craven. "Durability characterization of mechanical interfaces in solar sail membrane structures". *Advances in Space Research*, vol. 67, no. 9, pp. 2643–2654, 2021.

[19] "TU Delft Astrodynamic Toolbox", Accessed: 09 April 2024. URL `https://tudat-space.readthedocs.io/en/latest/index.html`.

[20] D. Dirkx, E. Mooij, and B. Root. "Propagation and estimation of the dynamical behaviour of gravitationally interacting rigid bodies". *Astrophysics and Space Science*, vol. 364, pp. 1–22, 2019.

[21] D. Dirkx, M. Fayolle, G. Garrett, M. Avillez, K. Cowan, S. Cowan, J. Encarnacao, C. Fortuny Lombrana, J. Gaffarel, J. Hener, et al. "The open-source astrodynamics Tudatpy software – Overview for planetary mission design and science analysis". *Europlanet Science Congress 2022*, vol. 16, no. 253, 2022.